Plasma Diagnostics Using K-Line Emission Profiles of Argon

Yiling Chen

Institute of Physics, University of Rostock, 18051 Rostock, Germany

Andrea Sengebusch

Institute of Physics, University of Rostock, 18051 Rostock, Germany

Heidi Reinholz

Institute of Physics, University of Rostock, 18051 Rostock, Germany

School of Physics, The University of Western Australia, WA 6009 Crawley, Australia

Gerd Röpke

Institute of Physics, University of Rostock, 18051 Rostock, Germany

Abstract

K-line profiles emitted from a warm dense plasma environment are used for diagnostics of Ar droplet plasmas created by high energy laser pulses. We observe temperature gradients within the Ar droplet from cold temperatures of the order of some 10 eV up to higher temperatures of about 170 eV. Non-perturbative wave functions are calculated as well as ionization energies, binding energies and relevant emission energies using a chemical *ab initio* code. The plasma screening is considered within a perturbative approach to the Hamiltonian. The plasma effect influences the many-particle system resulting in energy shifts due to electron-ion and electron-electron interaction. With this approach we get a good reproduction of spectral features that are strongly influenced by ionization and excitation processes within the plasma. Comparing with the widely known FLYCHK code, counting for internal degrees of freedom (bound states) and treating pressure ionization within our quantum statistical approach leads

Email address: andrea.sengebusch@uni-rostock.de (Andrea Sengebusch)

to different results for the inferred temperature distribution.

Keywords: plasma diagnostics, K line emission profiles, warm dense plasma, plasma polarization

---

1. Introduction

Plasma diagnostics using K_α fluorescence spectra allows to investigate properties of warm dense matter. This work focuses on the bulk temperature distribution of plasmas created from Ar droplets irradiated by high energy laser pulses with a power of 10^{19} W/cm^2, Ref. [1]. According to the high intensity, matter at temperatures between some 10 eV to 200 eV (bulk) and up to 1 MeV (blow-off) is created, so that most of the atoms are ionized and a wide range of different ion species is observed. To penetrate the plasma, the radiation frequencies ω have to be larger than the plasma frequency $\omega_{\mathrm{pl}} = \sqrt{\frac{n_e e^2}{\epsilon_0 m_e}}$, where n_e is the density and m_e is the mass of free electrons [2, 3]. The solid atomic density of Ar is $n_{\mathrm{tot}} = 2.636 \times 10^{22}$ cm^{-3}. Accordingly, free electron densities vary between $10^{22} - 10^{24}$ cm^{-3} depending on the ionization degree of the excited Ar plasma. Considering these free electron densities, x-rays are needed to investigate those plasmas. Due to laser plasma interaction the argon radiates K_α lines at 2957 eV and above, which can be used to infer the plasma parameters. To describe the plasma in the microscopic atomic region and its emission spectra as well, one has to consider in detail the influence of the plasma environment on the ionic potential, the electron-electron and the electron-ion interaction [4]. An electron is excited from E_0 (ground state) to E_i (initial state), and then, a photon is emitted in connection with the transition from E_i to E_f (final state). To describe the K_α emission spectra which corresponds to an electron going from the 2P to the 1S shell, the fine structure of the emitting state has to be considered. The creation of inner (K-) shell vacancies is accompanied by ionization and excitation of outer shell electrons (L- and M-shell) resulting in different satellite lines. Satellite energies significantly increase with the number of vacancies and excited states, respectively. The intensity ratio of different lines is determined

according to their statistical weight (LS coupling) and the abundance of corresponding emitters with respect to the plasma parameters. To introduce plasma effects, the electron-ion plasma screening is described within an ion sphere model approximation [4] and the electron-electron plasma screening is described within a quantum statistical approach by the Montroll-Ward self-energy contribution. Using coupled Saha equations, we consider the different charge states in thermodynamic equilibrium [3]. Finally, we add Lorentz profiles and convolute with a Gaussian instrument function to calculate synthetic spectra from the plasma shifted emission energies.

We compare our results with the experimental data presented in [1] as well as with theoretical results obtained with the FLYCHK code, also given in [1]. FLYCHK[5, 6, 7] provides emission spectra and ionization distributions within plasmas by solving rate equations for level populations considering collisional and radiative atomic processes. The code is well benchmarked for long-pulse laser experiments. However, there can appear jumps in the density of nearly neutral ion species if bound states are pressure ionized. When constructing synthetic X-ray spectra, line components that involve vanishing states have to be removed by hand if there is no steady fade out of its contribution with respect to the plasma parameters[8]. We apply an approach where pressure ionized states shift steadily into the continuum and no extra treatment is needed [9, 10].

2. Unperturbed emitter

2.1. Ionization energies

Solving self-consistent Roothaan-Hartree-Fock equations, we calculate the isolated ionic emitter energies using the chemical *ab initio* code Gaussian 03 [11]. The code was developed to perform molecular electronic structure calculations and is a powerful tool to determine the relevant binding, ionization and excitation energies for ions in different charge states.

The isolated, neutral Ar atom has 18 electrons bound to the nucleus. Removing stepwise the outer electrons, we look at ions up to the 14th ionization stage,

see Tab 1. Moreover, we do not only consider the ground state configurations but also some excited states of the ions. We found the aug-cc-pVTZ basis set [12, 13, 14] most suitable for the Ar system considered here. To show that G03 and the chosen basis set are reliable, we compare our calculated ground state ionization energies with different theoretical values in Tab. 2 and Fig. 1. N is the number of remaining electrons after ionization. The values for the emission energies differ only by some eV. The agreement is such, that the results in Fig. 1 can hardly be distinguished. The values in the table show that the ionization energy increases with increasing charge state of Ar. As the removed electrons can no longer screen the core, the remaining electrons are bound stronger and more energy is needed to remove the next electron. The kink at $N = 9$ is due to the fact that for larger N there are still electrons in the M-shell which are much less bound than L-shell electrons.

Fig. 2 shows the ionization energies for different charge states of Ar. Plotted again are the ionization energies of the ground state of the corresponding ions (in blue). Further, the black, green and red circles give results with valence electrons excited to 4s, 3d, 3p or 3s depending on the already reached charge state. For every ion we take into account up to 3 lowest excited states, additionally to the ground state. Tab 1 lists all the considered configurations before ionization. If we consider configurations with electrons excited to higher levels like 3d, these excited electrons are the ones to be removed by ionization. Hence we observe no kink at $N = 9$ but a smooth increase of ionization energy with rising charge.

2.2. Emission energies

The emission energies of the cold K_α doublet are found at about $\mathrm{K}_{\alpha_1} = 2958$ eV and $\mathrm{K}_{\alpha_2} = 2956$ eV [17]. This doublet describes the emission energy of the least excited and least ionized emitter. We compare our results for the K_α emission energies with other theoretical and experimental values to prove again the validity of our approach. We obtain an agreement with differences below 0.1%, see Tab. 3. Different K_α satellite emissions originate from different configurations of the emitting Ar ions. From Ar^+ to Ar^{9+} the ionization of the

ion	ground	exc. 3s	exc. 3p	exc. 3d	exc. 4s
Ar	$3s^2 3p^6$			$3s^2 3p^5\ 3d^1$	$3s^2 3p^5\ 4s^1$
Ar^+	$3s^2 3p^5$			$3s^2 3p^4\ 3d^1$	$3s^2 3p^4\ 4s^1$
Ar^{2+}	$3s^2 3p^4$			$3s^2 3p^3\ 3d^1$	$3s^2 3p^3\ 4s^1$
Ar^{3+}	$3s^2 3p^3$			$3s^2 3p^2\ 3d^1$	$3s^2 3p^2\ 4s^1$
Ar^{4+}	$3s^2 3p^2$			$3s^2 3p^1\ 3d^1$	$3s^2 3p^1\ 4s^1$
Ar^{5+}	$3s^2 3p^1$			$3s^2\ 3d^1$	$3s^2\ 4s^1$
Ar^{6+}	$3s^2$		$3s^1\ 3p^1$	$3s^1\ 3d^1$	$3s^1\ 4s^1$
Ar^{7+}	$3s^1$	$2p^6 3s^1$	$2p^6 3p^1$	$2p^6\ 3d^1$	
Ar^{8+}	$2p^6$	$2p^5\ 3s^1$	$2p^5\ 3p^1$	$2p^5\ 3d^1$	
Ar^{9+}	$2p^5$	$2p^4\ 3s^1$	$2p^4\ 3p^1$	$2p^4\ 3d^1$	
Ar^{10+}	$2p^4$	$2p^3\ 3s^1$	$2p^3\ 3p^1$	$2p^3\ 3d^1$	
Ar^{11+}	$2p^3$	$2p^2\ 3s^1$	$2p^2\ 3p^1$	$2p^2\ 3d^1$	
Ar^{12+}	$2p^2$	$2p^1\ 3s^1$	$2p^1\ 3p^1$	$2p^1\ 3d^1$	
Ar^{13+}	$1s^2 2s^2 2p^1$	$1s^2 2s^2 3s^1$	$1s^2 2s^2 3p^1$	$1s^2 2s^2 3d^1$	

Table 1: Considered outer shell configurations of ions before ionization.

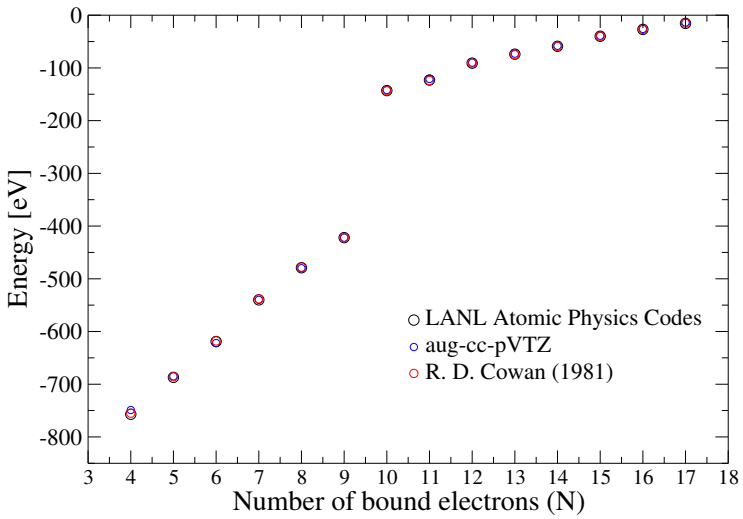

Figure 1: Ground state ionization energies for different charge states of Ar. N is the number of remaining electrons after ionization. Comparison of 3 different theoretical results, see Tab. 2.

ion	final config. $[1s^2 2s^2]$	this work [eV]	Cowan [eV] [15]	LANL [eV] [16]
Ar^{+}	$2p^6 3s^2 3p^5$	-14.57	-15.76	-15.56
Ar^{2+}	$2p^6 3s^2 3p^4$	-26.37	-27.63	-27.44
Ar^{3+}	$2p^6 3s^2 3p^3$	-39.39	-40.74	-40.47
Ar^{4+}	$2p^6 3s^2 3p^2$	-58.49	-59.81	-59.05
Ar^{5+}	$2p^6 3s^2 3p^1$	-73.93	-75.02	-74.71
Ar^{6+}	$2p^6 3s^2$	-90.30	-91.01	-91.26
Ar^{7+}	$2p^6 3s^1$	-121.88	-124.32	-123.22
Ar^{8+}	$2p^6$	-142.42	-143.46	-143.70
Ar^{9+}	$2p^5$	-422.56	-422.45	-422.15
Ar^{10+}	$2p^4$	-480.40	-478.69	-479.65
Ar^{11+}	$2p^3$	-540.25	-538.96	-540.12
Ar^{12+}	$2p^2$	-622.20	-618.26	-619.27
Ar^{13+}	$2p^1$	-685.36	-686.11	-686.28
Ar^{14+}		-749.41	-755.75	-757.33

Table 2: Calculated ground state ionization energies for different ionization stages.

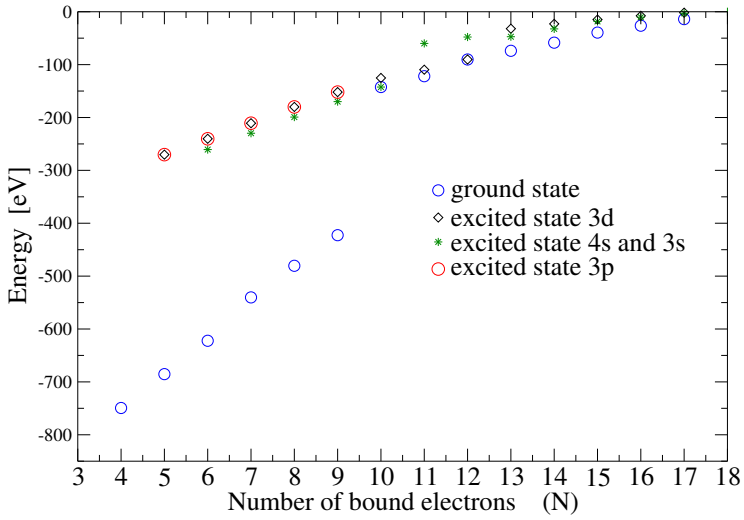

Figure 2: Ionization energies for different charge states of Ar. N is the number of remaining electrons after ionization. Different symbols show values for ground state and some excited state configurations according to Tab 1.

outermost electron occurs in the M-shell and emission energies vary only slightly from 2957 eV to 2970 eV. Then from Ar^{10+} to Ar^{14+} the L-shell is ionized and the emission energies rise sharply from step to step, see Tab. 4 and blue circles in Fig. 3. Tab. 4 shows also the initial configuration of the K_α transition for the ground state of the respective ion. To obtain the final configuration one electron has to be added in 1s ($1s^2$) and one has to be removed from 2p ($2p^6$ - $2p^0$). Analogously to the ionization energies, we also take into account excited emitter configurations with one valence electron in a higher shell (4s, 3d, 3p or 3s depending on the charge state). As a result we obtain emission energies similar to the ones where the valence electron is already ionized. Accordingly, the sharp rise in the emission energies of the excited states occurs one ionization step earlier than for the ground states, see Fig. 3.

Fig. 3 shows another interesting effect that needs further discussion: Looking at the distribution of the L-shell satellites we observe close lying Ar^{11+} ($N = 7$) and Ar^{12+} ($N = 6$) transitions. This is in contrast to the data shown by Neumayer *et al.*[1] where these states are more separated. The kink between

		K_{α_1} [eV]	K_{α_2} [eV]
P. Palmeri *et al.*[18]	Theo.	2958.70	2956.60
P. Palmeri *et al.*[18]	Theo.	2957.90	2955.90
P. Palmeri *et al.*[18]	Theo.	2957.68	2955.56
P. Neumayer *et al.*[1]	Exp.	2958.3	
NIST[17]	Exp.	2957.68	2955.56
this work	Theo.	2957.12	2955.11

Table 3: Different experimental and theoretical values for K_{α_1} and K_{α_2} of Ar^+.

ion	initial config. $[1s^1 2s^2]$	K_α [eV]	ion	initial config. $[1s^1 2s^2]$	K_α [eV]
Ar^+	$2p^6 3s^2 3p^6$	2957.12	Ar^{8+}	$2p^6 3s^1$	2966.70
Ar^{2+}	$2p^6 3s^2 3p^5$	2957.10	Ar^{9+}	$2p^6$	2969.03
Ar^{3+}	$2p^6 3s^2 3p^4$	2958.09	Ar^{10+}	$2p^5$	2993.08
Ar^{4+}	$2p^6 3s^2 3p^3$	2959.07	Ar^{11+}	$2p^4$	3017.96
Ar^{5+}	$2p^6 3s^2 3p^2$	2961.01	Ar^{12+}	$2p^3$	3023.01
Ar^{6+}	$2p^6 3s^2 3p^1$	2962.07	Ar^{13+}	$2p^2$	3054.59
Ar^{7+}	$2p^6 3s^2$	2965.65	Ar^{14+}	$2p^1$	3086.60

Table 4: Calculated ground state emission energies for different ionization stages.

$N = 7$ and $N = 6$ can be attributed to half-shell effects, which means for the K_α transition a half-filled shell in the final state ($2p^3$) but not in the initial state ($2p^4$) or a half-filled shell in the initial state ($2p^3$) but not in the final state ($2p^2$). Similar to closed shells also half-filled shells represent more stable states than configurations in between. The emission energy is the difference of the total energies of initial and final state. Hence, changes of the slope in the total energy of one of them create the observed kink. So the effect is clearly seen, however it might be overestimated by G03.

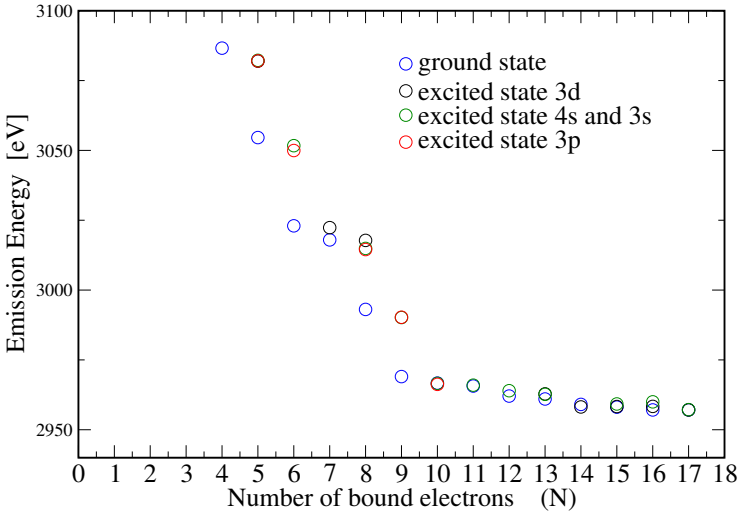

Figure 3: K_α emission energies for different charge states of Ar. N is the number of remaining electrons after ionization. Different symbols show values for ground state and some excited state configurations according to Tab 1.

3. plasma polarization

We add a plasma environment to the emitters and calculate shifts of the energy levels caused by the surrounding charges within a perturbative approach. To determine the distribution of the free plasma electrons around the quasi-static ionic emitters, an ion sphere or confined atom model is used [9]. The ion sphere contains a nucleus of charge $Z = 18$ and the respective number of electrons, so that the system in total is neutral. The electron density is distributed within the whole sphere and divided into the density of bound and free electrons. Accordingly, the radial Poisson equation for the potential $\phi(r)$ reads

$$\Delta\phi(r) = 4\pi e\ n_\mathrm{e}(r) + 4\pi e\ n_\mathrm{b}(r) - 4\pi Ze\ \delta(r). \tag{1}$$

The free electron density is determined self-consistently,

$$n_\mathrm{e}(r) \propto \int_{p_0}^{\infty} \frac{dp\ p^2}{(2mk_BT)^{3/2}} \exp\left[\left(\frac{-p^2}{2mk_BT} + \frac{e\ \phi(r)}{k_BT}\right)\right], \tag{2}$$

with the minimum momentum $p_0 = \sqrt{2me\ \phi(r)}$. The iteration starts with the potential where the free electron density is assumed to be constant throughout the sphere and follows

$$\phi(r) = -\frac{eZ}{2R}\left(3 - \frac{r^2}{R^2}\right), \tag{3}$$

with the Wigner-Seitz radius R which is the boundary of the ion sphere. We solve the radial Poisson equation iteratively and finally obtain a self-consistent free electron density which forms a polarization cloud close to the nucleus and dilutes for larger radii. Due to the screening of the free electrons the energy levels and hence the emission energies are shifted. We calculate these shifts in a first order perturbation theory approach to the Hamiltonian. As a result, shown in Fig. 4, we obtain line shifts to lower energies in the order of some eV depending on both the plasma temperature $k_B T$ and the average free electron density n_e. This effect is referred to as plasma polarization shift and can be explained as follows [9]: The free electrons screen the nucleus resulting in lower values of binding energies. As the 1s level is localized closer to the nucleus than 2p, it is more affected by the screening of the nucleus and thus experiences the larger shift. Since the emission energy is given by the difference of the two involved levels the spectral line is red shifted to lower energies. The red shift increases with rising free electron density as the screening of the nucleus rises as well. However, the red shift decreases with rising plasma temperature. This is due to the fact that the self-consistently determined free electron density within the ion sphere is not constant but radially dependent. A screening cloud of free electrons is formed around the nucleus and the density dilutes for larger radii. The higher the temperature the more this screening cloud is spatially extended ('smeared out') and the actual free electron density close to the nucleus decreases, resulting in a lower red shift.

4. plasma composition

Plasma polarization is not only important to calculate the accurate emission line positions but also to determine the plasma composition itself. In contrast to

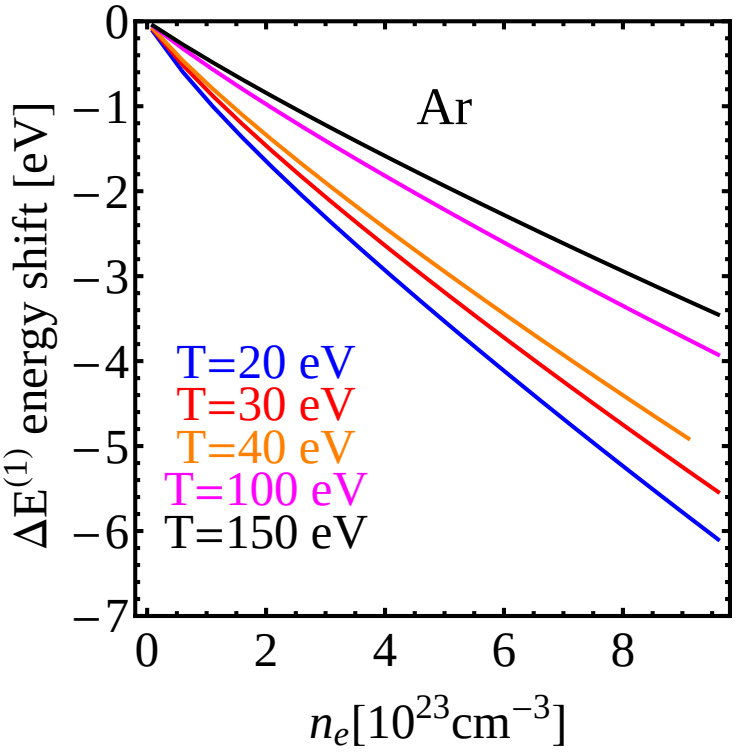

Figure 4: Shift of K_α emission energy with rising free electron density for different plasma temperatures.

emission lines, a single level surrounded by plasma is shifted to higher energies, i.e. closer to the continuum. Depending on the plasma parameters this shift can be that large that the continuum is reached and the bound electron is set free (pressure ionization, Mott effect [2]). Hence, we obtain another free electron and a new ion species. In the following we will outline how we calculated the plasma composition taking into account the polarization shifts we determined within the ion sphere model. For more details see again [9, 10].

Assuming a local thermal equilibrium, we apply Saha equations to determine the abundance of the different ion species,

$$\frac{n_{(m+1)} n_e}{n_{(m)}} = \frac{\sigma_e^{in}}{\lambda_e^3} \, \frac{\sigma_{(m+1)}^{in}}{\sigma_{(m)}^{in}} \; . \tag{4}$$

Here we use a representation of the chemical potential of species c which is of the same form as the one for the classical ideal gas, $\mu_c = k_B T \, \ln\left[\frac{n_c \lambda_c^3}{\sigma_c^{in}}\right]$. However, the internal partition function σ_c^{in} does not only contain the statistical weight but the particle interactions. Coupling the equations of successive ionization stages we obtain

$$n_{(m)} = \left[\frac{1}{n_e \lambda_e^3}\right]^m \; \sigma_e^{in}(m) \; \frac{\sigma_{(m)}^{in}}{\sigma_{(0)}^{in}} \; n_{(0)} \; . \tag{5}$$

Here, m denotes the m-th ionization stage with respect to the uncharged atom (reference state). Accordingly, $n_{(0)}$ and $n_{(m)}$ are the densities of particles in these states. Keeping the total particle density fixed at the bulk value the following conservation laws are used to solve the system of Saha equations

$$n_{\rm tot} = \sum_{m=0}^{Z} n_{(m)} \quad \text{and} \quad n_e = \sum_{m=0}^{Z} m \cdot n_{(m)} \; . \tag{6}$$

Here, we limit ourselves to a maximum number of ionization stages sufficient for temperatures we are interested in ($T \leq 180$ eV) , i.e. the sum doesn't run until 18 but is considered up to the boron like ion Ar^{13+}.

Let us now consider the electronic partition function σ_e^{in}. As for the electrons no internal degrees of freedom have to be taken into account, we split the partition function into the ideal part represented by the statistical weight and

a Boltzmann factor containing the interaction energy,

$$\sigma_e^{in} = g_e \; e^{-\Delta_e/k_B T} \; . \tag{7}$$

As we take into account different ionization stages the statistical weight of the m-th successive ionization step will add up to $g_e^m = 2^m$. The electron interaction energy Δ_e is treated as a rigid, momentum independent quasi-particle shift of the free particle energies and divided into an electron-ion interaction term and electron-electron interaction term. According to [9] the total internal partition function of the non-degenerate free electrons is given by

$$\begin{aligned} \sigma_e^{in}(m) &= 2^m \exp\left[-\frac{\Delta_e^{\mathrm{MW}}}{k_B T}\right]^m \\ &\quad \times \exp\left[\frac{1}{k_B T}\frac{e^2}{(4\pi)^{2/3}\epsilon_0}\left(\frac{n_e}{3}\right)^{1/3}\sum_{x=1}^{m} x^{2/3}\right]. \end{aligned} \tag{8}$$

For the contribution of the electron-electron interaction we use the Montroll-Ward approximation [3]

$$\begin{aligned} \Delta_e^{\mathrm{MW}} &= -\frac{e^2}{2}\sqrt{\frac{n_e e^2}{\epsilon_0 k_B T}} \\ &\quad + \frac{\sqrt{2\pi^2}\, n_e \lambda_e e^4}{8(k_{\mathrm{B}}T)^2} - \frac{n_e \lambda_e^3}{8\sqrt{2}} + \frac{n_e \lambda_e^2 e^2}{4 k_{\mathrm{B}} T}. \end{aligned} \tag{9}$$

For the internal partition functions of the ions $\sigma_{(m)}^{in}$ we have to consider internal degrees of freedom, i.e. differently excited bound states. The dynamical screening due to the plasma environment leads to a lowering of the ionization energies up to vanishing of bound states at the Mott densities (pressure ionization)[2]. Applying the Planck-Larkin renormalization the internal partition function for the m-th ionization stage reads as follows

$$\begin{aligned} \sigma_{(m)}^{in} &= \exp\left[-\frac{E_0^{(m+1)}}{k_B T}\right] \\ &\quad \times \sum_i \left(\exp\left[-\frac{\Delta E_i^{(m)}}{k_B T}\right] - 1 + \frac{\Delta E_i^{(m)}}{k_B T}\right) \; . \end{aligned} \tag{10}$$

To obtain this equation we separate the energies $E_i^{(m)}$ of possible bound states of the m-th ion into the ground state energy of the next ionization stage $E_0^{(m+1)}$

and possible excitations of the outermost valence electron $\Delta E_i^{(m)}$,

$$E_i^{(m)} = E_0^{(m+1)} + \Delta E_i^{(m)} \ . \tag{11}$$

Within this approximation a Mott transition would refer to a state where $\Delta E_i^{(m)} \to 0$ due to plasma polarization.

Keeping the total density fixed at the bulk value of $n_{\rm tot} = 2.636 \times 10^{22}$ cm^{-3} we calculate the abundance of different ion species (Fig. 5) and the corresponding average charge state (red circles in Fig. 6) in dependence on the plasma temperature. In Fig. 6, our charge state distribution is compared with results of Neumayer *et al.* [1] obtained from the FLYCHK code [1] (black dashed line, FWHM of charge state distribution in gray). We see a sharp rise of the charge state and a rapid sequence of ionization stages are passed through for temperatures below 40 eV. This is the regime of M-shell ionization, binding energies are rather low and pressure ionization plays an important role. Our results for the average ion charge match the upper FWHM of the charge state distribution of Neumayer *et al.*, i.e., at the same temperature our calculations give not only a higher charge state but also larger energy shifts of the emission energies.

The differences arise from the different treatment of the variety of bound states and pressure ionization within the approaches. As there are several hundred transitions closely distributed for lower charge states usually a simplification is applied for better handling. FLYCHK uses super-configuration transition arrays (effective bound states) weighted by respective transition rates rather than the complete level structure[1]. We do not average over several levels, but take only low lying excited states with rather high probability of occupation into account. Further, in the FLYCHK code continuum lowering is treated within a Stewart-Pyatt like model to implement medium corrections to the ionization energies. The model interpolates between the two limiting cases: Debye screening for dilute and hot plasma on the one hand and screening within an ion sphere model with constant free electron density for dense and cool plasmas an the other hand[7]. If bound states merge into the continuum the calculations get discontinuous since these states suddenly disappear from the implemented

rate equations. Using effective bound states reduces these events. Within our approach there is no such discontinuity thanks to the use of the Planck-Larkin renormalization of bound states.

As shown above we also use an ion sphere model to calculate the continuum lowering, however, the free electron density within the sphere is not constant but radially dependent. All in all we observe several Mott transitions in solid density Argon at temperatures below 50 eV which lead to a higher degree of ionization. Looking at Fig. 5 sodium, neon and flour like states seem to be rather stable. Hence, the slope of the charge state in Fig. 6 flattens for rising plasma temperatures from about 40 eV to 120 eV. Our results arrive at the values obtained by Neumayer *et al.* as the ion charges rise and pressure ionization becomes less important.

5. Synthetic spectra and temperature distribution

To construct synthetic spectra from the shifted emission energies every line as well as its fine structure components is assigned a Lorentz profile with natural line width γ and maximum intensity $I_{\max}$,

$$I(E) = \frac{I_{\max}\ (\gamma/2)^2}{(E - E_0)^2 + (\gamma/2)^2}\ . \tag{12}$$

The central line position E_0 is given by the plasma shifted line positions. Typically the $p_{3/2}$ component of the K_α transition provides the main contribution and we identify our emission energies obtained so far with these line components. To take into account fine structure splitting, we add the $p_{1/2}$ components semi-empirically. From NIST tables [17] it is known that the fine structure splitting of Ar K_α is 2.01 eV.

The maximum intensity is mainly given by the emitter abundance in the plasma. We determine all intensities relatively with respect to a reference state,

$$\frac{I_{\max}}{I_{\rm ref}} \simeq \frac{n}{n_{\rm ref}} \left(\frac{E_0}{E_0^{\rm ref}} \right)^4 . \tag{13}$$

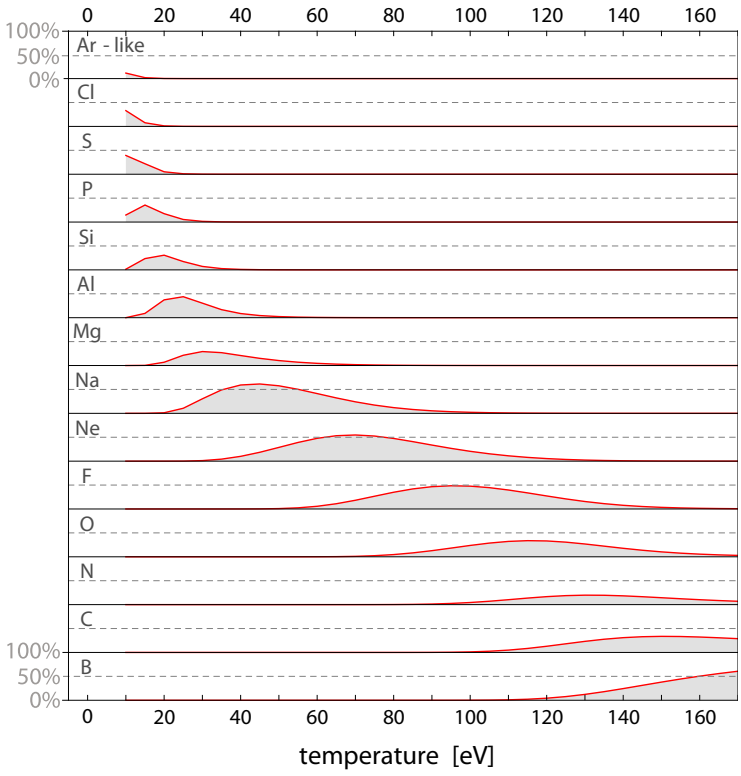

Figure 5: Plasma composition in dependence of bulk temperature: percental abundance of different Ar ions.

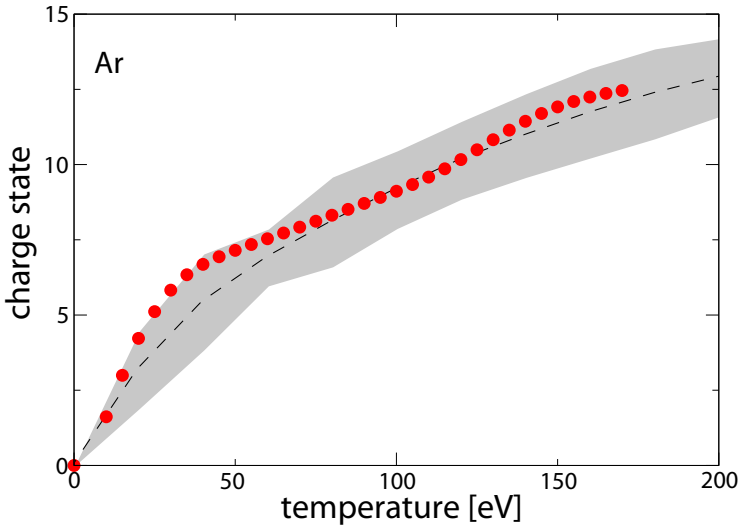

Figure 6: (circles, red) Average charge state of the plasma in dependence of bulk temperature. (dashed, black) Average charge state from Neumayer *et al.* obtained by FLYCHK[1]. (grey) FWHM of charge state distribution from Neumayer *et al.*[1]

For the electron transitions considered here, we assume nearly constant dipole matrix elements $\left|\frac{1}{\Omega_0}\int d^3r\ \varphi^*_{\rm in}\ \vec{r}\ \varphi^*_{\rm fin}\right|^2$ with respect to excitation and ionization of outer shells since the one particle wave functions $\varphi_{\rm in}$ (initial state, 2p) and $\varphi_{\rm fin}$ (final state, 1s) change only very slightly [10]. Hence, the Einstein coefficients for spontanious emisssion is simply $\propto E_0^3$.

The Lorentzians are summed up and convoluted with a Gaussian profile of width Γ to take into account instrumental broadening of the measurements.

According to Neumayer *et al.* [1] we varied the broadening parameters within the range of some eV and found the most suitable combination in a natural linewidth of $\gamma = 1$ eV and a Gaussian width of $\Gamma = 3$ eV. A selection of spectra for different plasma temperatures is shown in Fig. 7. Keeping the total density and plasma temperature fixed, the free electron density is given by the composition calculations. Shown are some typical spectra: At low temperatures up to some 10 eV we are again in the regime of M-shell ionization. Since the emission energies vary only slightly the lines of from Ar^+ to Ar^{9+} group within

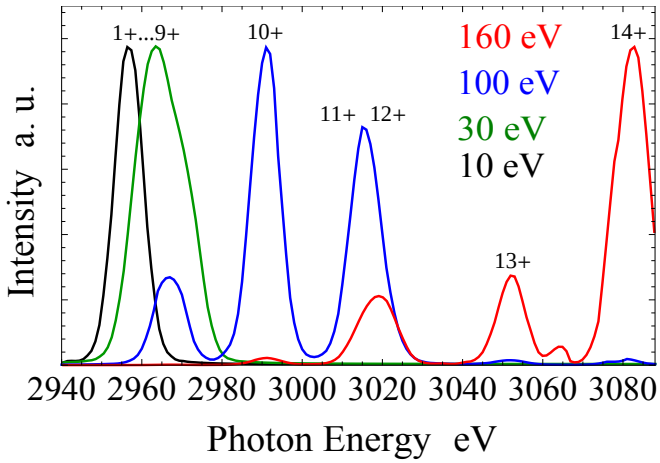

Figure 7: Selected normalized synthetic spectra for four different plasma temperatures. The total density is fixed at the bulk value, the free electron density corresponds to the plasma composition.

one large main peak which shifts to higher energies with rising temperatures. With further increase of the temperature we enter the regime of L-shell ionization, the main peak becomes less prominent and several distinguishable peaks appear corresponding to the separated emission energies of the respective ions. We calculated spectra up 160 eV where the last L-shell satellite is dominant.

Experimentally observed higher emission energies mainly arise from ions with only one or two electrons (Ly-α, He-α, intercombination line) and represent the conditions of the blow-off plasma instead of bulk properties.

We apply a superposition of our spectra for different temperatures to model the experimental results obtained by Neumayer *et al.* [1]. To obtain the best fit the weight of the different spectra is determined within a variational approach using the method of least squares. Results for the best fit and the corresponding temperature distribution are shown in Fig. 8 and Fig. 9, respectively.

The superimposed spectrum shows a good agreement especially for the M-shell satellites. The position of the main peak is rather sensitive to the plasma temperature. The nearly same contribution of 20 eV and 30 eV and the slightly

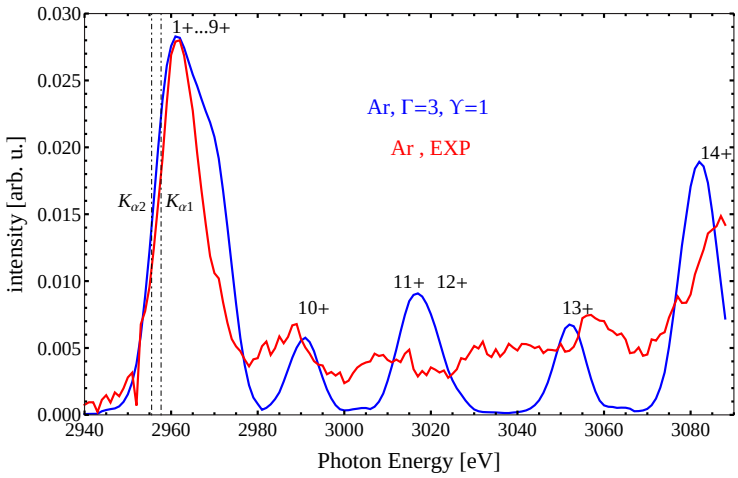

Figure 8: Best fit of superposition of theoretical spectra and space-time-integrated measurements of Neumayer *et al.* [1].

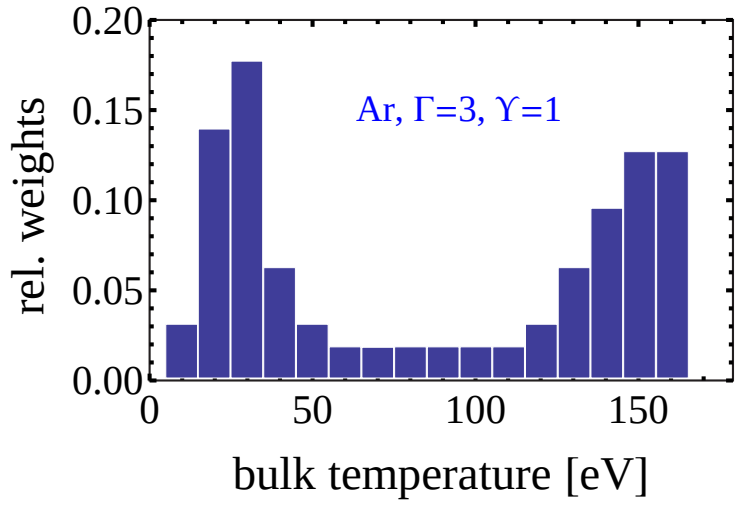

Figure 9: Temperature distribution which gives the best fit of theoretical and experimental spectra. The relative weights are determined via the method of least squares.

overestimated width in Fig. 8 suggest an intermediate temperature of about 27 eV to best represent the M-shell peak. At a first glimpse the agreement with the L-shell satellites is less satisfying. The peaks are at correct positions but the widths seem to small. We attribute this to our approximation of the natural line widths. We use a single value of γ which implies the same lifetime for all considered states. But especially highly ionized and excited states experience shorter lifetimes and hence show a larger natural width. Accordingly the L-shell emission lines would blur and give a better fit of the energy spectrum above 2980 eV.

6. discussion and conclusion

The temperature distribution we obtain is similar to the theoretical results of Neumayer *et al.*[1]: a two-peaked curve with the first focus at lower temperatures of some 10 eV, the second focus at more than 100 eV higher temperatures and a less pronounced region in between. However, there is a significant difference between the distribution of Neumayer *et al.* and the results shown here: our first focus lies at about 20 eV lower plasma temperature. This difference is due to the different results of the composition calculations. The results for undisturbed peak positions are rather the same, showing blue shifted emission energies as described above. But as we obtain higher degrees of ionization at lower temperatures, we also see the blue shift of emission energies at lower temperatures and hence we obtain a temperature of about 27 eV instead of 50 eV to fit the main peak of the measured spectrum. Neumayer *et al.* discussed several mechanisms like resistive heating or radiative heating that might help to explain the absence of temperatures below 50 eV. However, our results suggest that these influences might not be as substantial as the authors assumed.

We see that the details of the synthetic spectra need further discussion. Firstly, the unperturbed spectra calculated by different approaches here and in Ref.[1] show differently distributed transitions for the L-shell excitations. Our close lying Ar^{11+} and Ar^{12+} states are in contrast to the data used by Neumayer

et al. where these states are more separated. Secondly, the distribution of transitions as a function of the energy is broader in Ref.[1] so that the L-shell peaks in the final spectrum merge. Whereas we obtain clearly separated structures. The calculation of atomic states and transitions is a question of the used codes and surely needs special consideration in future works.

Furthermore, the broadening of the lines is different in both approaches. Using the same parameter values for the broadening of all lines overestimates the width for the main peak (Ar^{+} to Ar^{9+}) and underrates the width for the higher lying peaks as pointed out above. A more detailed discrimination of the widths would improve the agreement between theory and experimental data. In particular, the low minima between the theoretical peaks will possibly be smeared out. A quantum statistical approach to the line width would be desirable which is well elaborated for H-like systems but needs further development for mid-Z materials.

The inclusion of plasma effects, especially shifts and the merging of bound states with the continuum, is important to discuss the composition of the plasma and the density of free electrons. We have shown that such effects have significant influence on the inferred temperature distribution. However, in order to describe the origin of the inferred temperature profile, kinetic codes and hydrodynamic simulations are inevitable. In general we have shown that K-alpha spectroscopy is an interesting means for plasma diagnostics and allows an estimate of the temperature profile in warm dense matter.

Acknowledgements

We would like to thank P. Neumayer for fruitful discussions and the experimental data. This work has been supported by the German Research Foundation through the Collaborative Research Center 652 - Strong correlations and collective effects in radiation fields: Coulomb systems, clusters and particles.

References

References

[1] P. Neumayer, B. Aurand, R. A. Costa Fraga, B. Ecker, *et al.*, Phys. Plasmas 19 (2012) 122708.

[2] W.-D. Kraeft, D. Kremp, *et al.*, Quantum Statistics of Charged Particle Systems, Verlag Berlin, 1986.

[3] D. Kremp, W.-D. Kraeft, *et al.*, Quantum Statistics of Nonideal Plasmas, Springer Berlin, 2005.

[4] D. Salzmann, Atomic Physics in Hot Plasmas, Oxford University Press, Inc, 1998.

[5] H.-K. Chung, M. Chen, W. Morgan, Y. Ralchenko, R. Lee, HEDP 1 (2005) 3.

[6] Flychk at nist, online database.
URL http://nlte.nist.gov/FLY/

[7] H. K. Chung, R. W. Lee, M. H. Chen, Y. Ralchenko, The How To For FLYCHK at NIST, 2008, (user manual).
URL http://nlte.nist.gov/FLY/Doc/Manual_FLYCHK_Nov08.pdf

[8] E. Stambulchik, V. Bernshtam, L. Weingarten, E. Kroupp, *et al.*, J. Phys. A: Math. Theor. 42 (2009) 214056.

[9] Y. Chen, A. Sengebusch, H. Reinholz, G. Röpke, Contrib. Plasma Phys.In print.

[10] A. Sengebusch, H. Reinholz, G. Röpke, U. Zastrau, *et al.*, J. Phys. A: Math. Theor 42 (2009) 214061.

[11] M. J. Frisch, *et al.*, gaussian 03 (revision c.02) (Wallingford, CT: Gaussian Inc.) (2004).

[12] H. B. Schlegel, M. J. Frisch, Int. J. Quant. Chem. 54 (1995) 83–87.

[13] D. E. Woon, T. H. Dunning, J. Chem. Phys. 98 (1993) 2.

[14] R. A. Kendall, T. H. Dunning, J. Chem. Phys. 96 (1992) 6796.

[15] R. D. Cowan, The Theory Of Atomic Structure And Spectra, University of California Press, 1981.

[16] Los alamos atomic physics codes, online database.
URL http://aphysics2.lanl.gov/tempweb/lanl/

[17] Nist x-ray transition energies database, online database.
URL http://www.nist.gov/pml/data/xraytrans/

[18] P. Palmeri, P. Quinet, *et al.*, The Astrophys Journal Supplement Series 177 (2008) 408–416.